Structural Dimorphism of Bile Salt/Lecithin Mixed Micelles. A Possible Regulatory Mechanism for Cholesterol Solubility in Bile? X-ray Structure Analysis†

Karl Müller*

ABSTRACT: The three-dimensional structure of bile salt/lecithin mixed micelles in 0.15 M saline was derived from X-ray small-angle scattering measurements under various conditions. Two essentially different types of micelles were detected. At bile salt:lecithin molar ratios lower than approximately 2:1, lamellar particles similar to a lecithin bilayer arrangement were found. The thickness of the bilayer is 5.1 nm for mixed micelles having a molar ratio of 1:1. The lateral dimensions of the micelle were found strongly dependent upon molar ratio, increasing as lecithin content increases. In addition, it appeared that under certain incompletely defined conditions vesicular particles having diameters in the region of more than 100 nm occur. A molecular model of this type of micelle has been derived by means of a thorough interpretation of the electron density distribution across the plane of the bilayer. This model is generally consistent with the "mixed-disk" model of Mazer et al. [Mazer, N. A., Kwasnick, R. F., Carey, M. C., & Benedek, G. B. (1977) *Micellization, Solubilization, Microemulsions, Proc. Int. Symp. 1*, 383–402] and thus differs from that proposed by Small [Small, D. M. (1967) *Gastroenterology 52*, 607–610] and Dervichian [Dervichian, D. G. (1968) *Adv. Chem. Ser. No. 84*, 78–87]. At molar ratios exceeding 2:1, a different type of micelle structure was found. This is a highly isometrical particle of globular shape, probably having a centrosymmetric arrangement of the molecular constituents. At a 3:1 bile salt:lecithin molar ratio, the mean physiological ratio for human gallbladder bile, the diameter of this micelle is 6.2 nm. Provided that other bile constituents have no significant influence on the structure, it may reasonably be expected that native gallbladder bile contains micelles of this latter type. The prevalent balance between the two micellar forms may thus regulate the capacity of bile to transport cholesterol.

Cholesterol cholelithiasis is a widespread disease in western developed countries (Ingelfinger, 1968), and numerous studies have been carried out to clarify its etiology (Admirand & Small, 1968; Nilsson & Scherstén, 1969; Small & Rapo, 1970; Vlahcevic et al., 1971; Grundy et al., 1972; Northfield & Hofmann, 1975; Shaffer & Small, 1977). The essential outcome of these studies was that supersaturation of bile with cholesterol is necessary for cholesterol precipitation and consequent gallstone formation. The degree of supersaturation was usually estimated from the phase diagrams of Bourgès et al. (1967). These had been constructed from cholesterol solubility studies of model systems composed of bile salt, lecithin, and cholesterol, which together amount to ~80% of the total solids of bile.

In most of the work cited above, this line of argument was taken one step further. Supersaturation was thought to be not only the necessary but also an entirely sufficient requirement for stone formation. Supersaturated bile was inevitably considered to be lithogenic.

There is now reason to think that this is not the case. Holzbach et al. (1973) found that nonlithogenic bile is frequently supersaturated with cholesterol. Carey & Small (1978), who gave an improved definition of the degree of saturation by relating the maximum cholesterol solubility to the total lipid concentration, found that the bile of about half of the normal subjects also showed considerable cholesterol supersaturation. These studies lead to the postulate that, while cholesterol supersaturation is an essential prerequisite for stone formation, other factors may mediate stability or precipitation. The aim of the present studies has been to determine whether such factors exist and how they act in human bile.

Cholesterol is solubilized in bile by incorporation into mixed micelles (Carey & Small, 1970) formed by the two major constituents, bile salts and lecithin. The molecular arrangement of these micelles is obviously of great importance for their ability to solubilize cholesterol. Despite a number of previous studies (Small et al. 1969; Shankland, 1970, 1977; Stevens, 1977; Gähwiller et al., 1977; Oh et al., 1977; Mazer et al., 1977), essential features of the molecular architecture have remained obscure. This is largely because the methods used yield little direct information about the structure of the micelle. These methods can therefore only allow the structure to be inferred. Direct information on micellar structure can be derived, however, from X-ray small-angle scattering (XSAS). Apart from a single study by Fontell (1971) which concentrated only on simple bile salt micelles, no XSAS analysis on this subject has previously been published.

A widely accepted model for the structure of the biliary mixed micelle has been that proposed by Small (1967), which was found compatible with NMR data (Small et al., 1969). It consists of a disk-shaped bilayer of lecithin molecules surrounded at its perimeter by bile salts, so that the hydrophobic faces of the bile salts are in contact with the fatty acid chains of the phospholipids, while the bile salt hydroxyl groups are exposed to the aqueous environment. In spite of the plausibility of this model, we demonstrate below that it is not valid. The "mixed-disk" model of Mazer et al. (1977) is supported by the present analysis but with one very important reservation: it holds only for lecithin-rich micelles with lecithin to bile salt molar ratios greater than 0.55:1. For gallbladder bile, in which by contrast the micelles are bile salt rich, on the basis of present data, a new model is presented.

† From the Institut für Röntgenfeinstrukturforschung, der Österreichischem Akademie der Wissenschaften und des Forschungszentrums Graz, A-8010 Graz, Austria. *Received September 19, 1980.* This work was generously supported by the Österreichischer Fonds zur Förderung der Wissenshaftlichen Forschung. Partial support was also provided by National Institutes of Health Grant AM-17562.

* Present address: Sterling Laboratory of Chemistry, Yale University, New Haven, CT 06510.

0006-2960/81/0420-0404$01.00/0

The X-ray small-angle scattering (XSAS) method, in addition to the great advantage of yielding information on internal structure, also yields information on particle size, mass, and shape. In the present work, data on all of these structural parameters are derived from applications of this method to bile salt–lecithin micelles. The possibilities of XSAS in the investigation of complex particle structures in aqueous solution have been demonstrated by studies on serum lipoproteins (Müller et al., 1978; Laggner & Müller, 1978). Another advantage of XSAS as compared to hydrodynamic methods, including quasi-elastic light scattering, is that the data are much less affected by interparticle interactions and by hydration phenomena. The influence of these effects which are of particular importance for the present case of charged micelles formed by amphiphiles can be unambiguously determined and thus taken into account in the data analysis.

Materials and Methods

Bile salts used for the preparation of mixed micellar solutions were purchased from Sigma Chemical Co., St. Louis, MO, and were of 95% purity as indicated by thin-layer chromatography (Chavez & Krone, 1976). This is considered an adequate degree of purity for structural studies [though not for cholesterol solubility studies, in which heterogeneous nucleation may play an important role (Carey & Small, 1978)]. Therefore, the bile salts were used without further purification.

Egg-yolk lecithin was obtained from Lipid Products, South Nutfield, U.K., and was pure by thin-layer chromatography standards. A molecular weight of 770 was taken for calculating molar mixing ratios according to the average fatty acid composition of egg-yolk lecithin (Small et al., 1966a).

The micellar solutions were prepared by mixing appropriate volumes of methanol stock solutions of bile salts and chloroform/methanol stock solutions of lecithin. The mixtures were dried with a stream of nitrogen, residual solvent was removed by vacuum, and the coprecipitate was dissolved in bidistilled water containing 0.15 M NaCl adjusted to pH 9 by NaOH. All the micellar solutions were clear and colorless.

We used a physiological mixture of dihydroxy and trihydroxy bile salts in a 1:1 ratio, with a ratio of glycine to taurine conjugates of 2:1 (Neiderhiser & Roth, 1968; Hofmann & Small, 1967). However, the choice of bile salt species was found to have essentially no influence on the results. (Ursodeoxycholate has not yet been studied.)

X-ray Measurements. Cu radiation was obtained from a modified (Jânosi & Degovics, 1976) Rigaku Denki RU 500 generator with a rotating anode operating at 50 kV and 400 mA. A line-shaped primary beam, 25 × 2.5 mm, was formed in the plane of registration with a total intensity of 8×10^7 pulses/s.

The measurements were carried out with the use of a slit camera with a collimation system according to Kratky (1954). The modified camera type employed in this work (the so-called "compact camera") was based on a novel design by Stabinger & Kratky (1979) and differed in several particulars from the well-known previously described model (Kratky, 1958; Kratky & Skala, 1958). Important modifications in design include the following:

(1) The collimation system is mounted in a fixed position relative to the anode-terminal side of the X-ray tube so that shifts of the focus relative to the collimation system caused by temperature fluctuations are avoided. This is not the case when the camera is mounted in front of the X-ray tube. In fact, a considerably higher stability of the intensity is achieved by this arrangement as compared with the conventional one. Moreover, the alignment of the camera is strongly facilitated.

(2) The bridge of the collimation system has side bars directed toward the X-ray tube which are ground and lapped together with the lower side of the bridge. The remaining part of the collimation system is pressed from below against these side bars. By reason of simple geometrical considerations, imperfections in grinding and fit of the bridge are now of much less influence than has previously been the case with the conventional arrangement. Conventionally, the bridge is mounted on side bars of the middle edge which are directed off the X-ray tube.

(3) The camera is evacuated throughout from the entrance of the beam into the collimation system up to immediately before the counter slit. Parasitic scattering as it is generated from two sources in the conventional system is thus eliminated. These are, first, the foil closing the evacuated collimation system in front of the sample and, second, the foil closing the window of the vacuum tube separating the sample from the counter slit.

(4) The sample is situated within the vacuum in the new model. The sample holder which is equipped with a Mark capillary for use with liquid samples can be inserted and removed from the side face of the camera without opening the vacuum-tight cover. The capillary is fastened in the sample holder so that it is protected against fracturing. Also, it is open at both ends in order to facilitate cleaning and to allow measurements in the flowing-through mode. Since both ends can be liquid and vacuum tight sealed, normal use with static liquids is also possible.

(5) Counter slit and counter tube are moved together, whereas the vacuum tube is in a fixed position. This is to avoid impairment in precision of the sensitive mechanics for the movement of the counter slit resulting from the weight of the vacuum tube. For exposure, the samples were held in glass capillaries (Hilgenberg, Malsfeld, Germany) which were 0.1 cm in diameter and had 0.001 cm walls. A constant temperature of 37 ± 0.1 °C was maintained by an electronically controlled Peltier cuvette (Leopold, 1969). The scattering curves were registered in the step scanning mode in a range of $0.10\ \text{nm}^{-1} < h < 5.5\ \text{nm}^{-1}$, corresponding to scattering angles of $\sim 2.5 \times 10^{-3}$ to $\sim 1.5 \times 10^{-1}$ radians ($h = (4\pi/\lambda) \sin\theta$, 2θ is the scattering angle). To minimize the effects of equipment instability, eight scans of each scattering curve were recorded and averaged. A total of 2×10^5 pulses were collected at each of the 120 points of every scan. A blank scattering curve for the solvent-filled capillary was determined under identical conditions. A pulse-height discriminator was used to selectively record the Cu K energy range, and the influence of Cu Kβ radiation was taken into account mathematically by a deconvolution method (Glatter, 1977).

Density Measurements. The apparent partial specific volume of the scattering particles, ϕ', was derived from high prescision density measurements ($\pm 10^{-6}$ g·cm^{-3}) performed with an Anton Paar DMA 60 digital density meter (Kratky et al., 1973), equipped with two external measuring cells 601 operating in the phase locked loop mode (differential densimetry) for minimzation of the influence of temperature fluctuations. ϕ' was calculated from the observed densities according to

$$\phi' = d_1^{-1}[1 - (d_2 - d_1)c^{-1}] \quad (1)$$

(d_1 = density of the solvent; d_2 = density of the solution; c = concentration of solute in g·cm^{-3}). ϕ' values varied by not more than 1% when diluting the micellar solutions from 10% to 1% (w/v) and not more than 2% when varying the NaCl content from 0 to 0.15 mol/L. Accordingly, these apparent values sufficed for calculation of electron density differences and

micelle molecular weights, without need for precisely defining the preferential interactions in a multicomponent solvent system (Casassa & Eisenberg, 1964).

Data Evaluation. The first important step is calculation of the particle scattering function from the measuring data from the scattered radiation. This requires eliminating the smearing effect caused by the finite size of the primary beam, eliminating residual effects of polychromaticity, and smoothing statistical noise. These operations can be carried out elegantly and accurately by the recently developed method of Indirect Fourier transformation (Glatter, 1977), which, in addition, yields the electron pair distance distribution function $p(r)$, which is defined as

$$p(r) = \frac{1}{2\pi}\int_0^\infty i(h)h^2\frac{\sin hr}{hr}\,dh \qquad (2)$$

and yields the number of the individual electron pair distances within the particle.

The traditional way of calculating $p(r)$ has been to compute the Fourier transform of the experimental scattering curve, but this process is subject to several major sources of errors: termination of the data at large and small angles, statistical noise, background scattering, and concentration-dependent interparticle interference effects. All of these give rise to large oscillations in $p(r)$. These are superimposed upon the intrinsic structural information contained in $p(r)$ and, in most cases, prevent an accurate evaluation of this function. Indirect Fourier transformation circumvents this problem in the following way: a hypothetical $p(r)$ function is generated in real space by addition of a set of auxiliary spline functions. These functions are Fourier transformed into reciprocal space and adjusted by a least-squares algorithm to obtain an optimum fit to the experimental data. The adjusted splines then yield the correlated $p(r)$ function in real space. The power and validity of this approach have been tested extensively with several hundred experimental and theoretical scattering curves and have been documented in a number of communications (Müller et al., 1978; Laggner & Müller, 1978; Laggner et al., 1977).

Once $p(r)$ has been determined, structural parameters can be obtained.

(a) The maximum particle dimension, D, is the point at which $p(r)$ becomes zero.

(b) The radius of gyration, R, is calculated from the second moment of $p(r)$ according to

$$R^2 = \frac{\int_0^\infty p(r)r^2\,dr}{2\int_0^\infty p(r)\,dr} \qquad (3)$$

Calculation of R in this way was shown (Glatter, 1977) in many practical examples to be more reliable than the traditional Guinier method.

(c) The scattered intensity at zero angle, $i(0)$, as needed for molecular weight calculation:

$$i(0) = \int_0^\infty p(r)\,dr \qquad (4)$$

Since $p(r)$ is an integral function over the entire angular range of the scattering curve, a higher accuracy is achieved by using relation 4 than by extrapolating the innermost scattering points to zero angle.

(d) Since artificial oscillations are avoided by the indirect transformation method, the internal electron density distribution can be determined from the trace of the $p(r)$ function. For symmetrical structures, this can be done by direct deconvolution of $p(r)$.

(e) The particle shape is reflected by the course in the outer part of $p(r)$, and a clear distinction between isometric particles and various types of anisometric particles can be made (Glatter, 1979a; see also Figures 8 and 9).

(f) The effects of interparticle interference at finite concentration can be estimated and eliminated by extrapolation to zero concentration in a defined way (see also Figures 2 and 3).

(g) The influence of background scattering caused by random short-range electron density fluctuations within the particle is restricted to an increase in the $p(r)$ function at smallest r values and can easily be eliminated by subtraction of a constant term from the scattering curve so that $p(r)$ reaches zero at $r = 0$.

Results and Discussion

Scattering curves were recorded for a series of bile salt:lecithin molar ratios ranging between 6:1 and 1:1.5. Substitution of dihydroxy for trihydroxy bile salts, taurine for glycine conjugates, or the physiological mixture of six naturally occurring bile salts for a single bile salt species produced no significant differences in the scattering curves.

Essential differences, however, were observed when a critical bile salt to lecithin ratio was exceeded. At bile salt:lecithin ratios lower than approximately 2:1, micelles with a bilayer arrangement of the constituents were found. In what follows, we shall designate these micelles as the "lecithin-rich type". In contrast, if a mixing ratio of 2:1 was exceeded, a quite different molecular architecture was detected which has not previously been described in the literature. We shall subsequently refer to these as the "bile-salt-rich type" of mixed micelles. Since the characteristic structural features of these two different types are not essentially dependent upon mixing ratio beyond the 2:1 transition point, the description for each case will be confined to one representative, i.e., a 3:1 bile salt/lecithin system for the bile-salt-rich type and a 1:1 bile salt/lecithin system for the lecithin-rich type, respectively.

Figure 1 shows the scattering curves and distance distribution functions for these two mixtures. These data led to the results given below.

Micelle Molecular Weight. The molecular weight of a scattering particle can be determined according to

$$M = i(0)^{1/2}(\Delta z)^{-1} \qquad (5)$$

(Kratky, 1963), where

$$\Delta z = (z_2 - z_1)d_1\bar{v}_2 \qquad (6)$$

The scattered intensity $i(0)$ of a single particle (Luzzati, 1960) is related to the experimentally determined intensity $I(0)$ at zero angle by

$$i(0) = KI(0) \qquad (7)$$

and

$$K = Ma^2/(P_0I_eN_AcD) \qquad (8)$$

(z_1, z_2 = electron concentration of the solvent (1) and the solute (2) in mol-electrons/g; d_1 = density of the solvent in g/cm^3; $\bar{v}_2$ = partial specific volume of the solute in cm^3/g; a = distance from the sample to the plane of registration in cm; P_0 = intensity of the primary beam in counts/s; I_e = Thomson scattering factor of a single electron; M = particle mass in g/mol; N_A = Avogadro's number; c = solution concentration in g/cm^3; D = thickness of irradiated sample in cm).

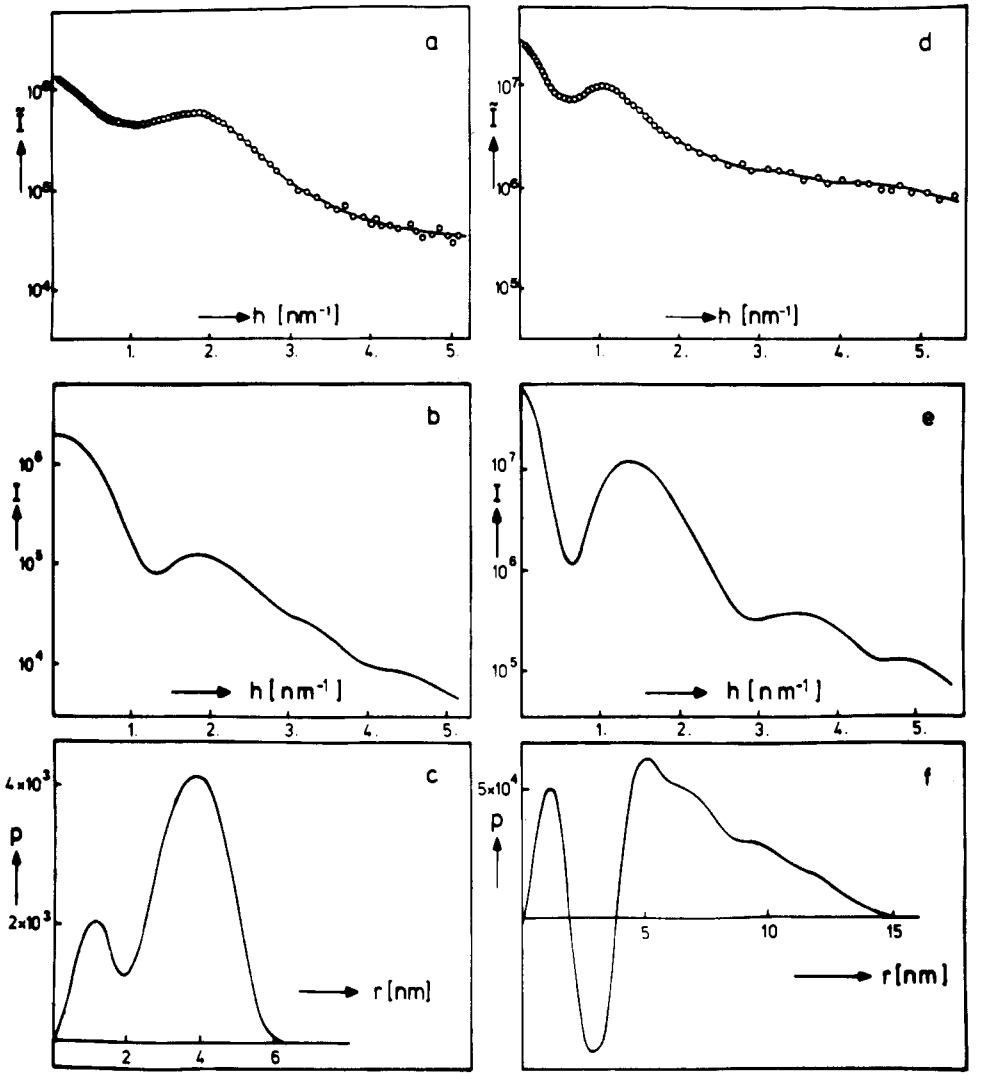

FIGURE 1: Experimental measuring points of the 3:1 (a) and 1:1 (d) mixed micelles. The full line is the approximated scattering function obtained by Fourier transformation of the distance distribution function convoluted with the primary beam profiles (length and width) and the wavelength profile. Parts b and e are the respective scattering functions (without collimation errors) extrapolated to zero concentration. The corresponding distance distribution functions are shown in (c) and (f).

In a multicomponent system as represented by the one in our study, the value of $\bar{v}_2$ in eq 6 is to be replaced by an expression containing the preferential interaction terms. This was not done here because the difference was shown to be very small (Casassa & Eisenberg, 1964; Kupke, 1973; Lee & Timasheff, 1974).

For 3:1 micelles at 37 °C in 0.15 M NaCl, we found the following values: 0.885 at 10%, 0.880 at 5%, 0.878 at 2.5%, and 0.877 at 1.25% (all w/v). Since the structure of this bile-salt-rich complex was found to be practically independent of dilution in this range, a value of 0.875 cm^3/g was obtained for ϕ_2' by extrapolation to zero concentration.

Since the 1:1 system depends considerably on the actual concentration, only the apparent specific volumes at finite concentration can be obtained. These are 0.912 (10%), 0.915 (5%), 0.918 (2.5%), and 0.919 (1.25%). The corresponding values for the molecular weight are therefore of lesser accuracy.

On the basis of chemical composition, the electron concentrations, z_2, were 0.5463 and 0.5508 mol-electron/g, respectively, for the 3:1 and 1:1 particles.

Applying eq 4, 5, 6, and 7, a micellar weight of 27 000 ± 10% was found for the 3:1 mixed micelles, corresponding to aggregation numbers of 36:12. For the 1:1 case, a micellar weight of 250 000 ± 30% was obtained, corresponding to aggregation numbers of 200:200. These aggregation numbers were calculated on the assumption that the bile salt molecules all form mixed micelles, with no coexisting simple bile salt micelles. This assumption will be justified below.

Maximum Dimensions of the Micelles. As briefly described in the section Data Evaluation, D can be obtained from the distance distribution function without complications caused by concentration effects. In Figure 2 we demonstrate this for the example of a spherical particle with a shell that is more dense than its core. This particle is similar to the 3:1 micelle, as we subsequently show.

Parts a and b of Figure 3 show the concentration dependence of the 3:1 experimental scattering curves and the corresponding curves for $p(r)$. The maximum dimension of the 3:1 micelles is 6.2 ± 0.2 nm. The shape of $p(r)$ as well as D determined from the position of the trough remains practically unchanged. This indicates that for 3:1 micelles dilution does not cause a detectable micellar growth. This can be explained by the small dependence of the size of bile-salt-rich micelles on the mixing ratio. In preliminary experiments, it was found that the diameter of a pure bile salt micelle of about 5.5 nm increases almost linearly up to 6.4 nm at the critical mixing ratio of 2:1. Dilution with 0.15 M saline from 10% to 1.25% is accompanied by a shift of the intramicellar mixing ratio from 3:1 to approximately 2.75:1 because additional bile salt is needed to

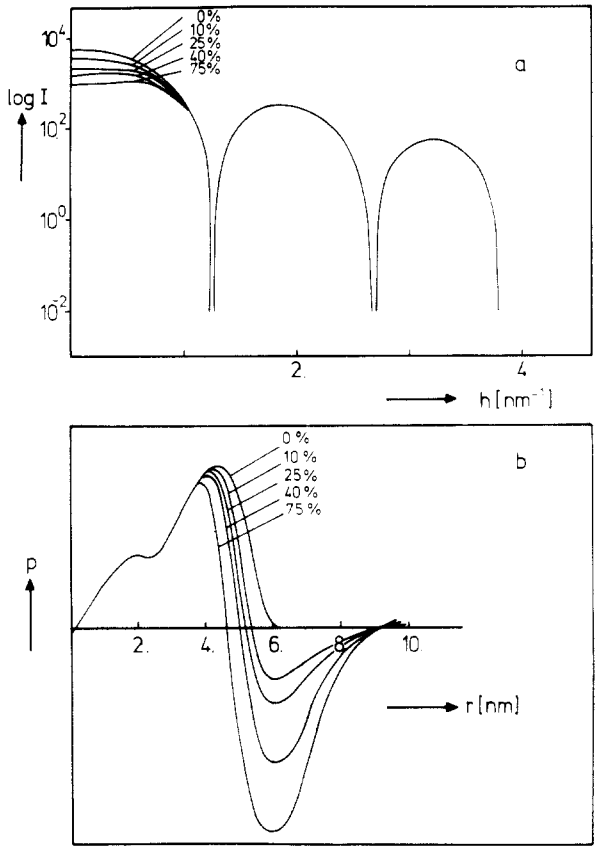

FIGURE 2: Model calculation of the interparticular interference effect based on hard sphere interaction between spherical particles constructed similar to the structure found for the 3:1 micelles (core-shell electron density distribution; 6-nm diameter). The numbers in the upper figure indicate the actual concentration (w/v). As becomes evident from part b, the position of the negative trough remains constant and coincides with the true diameter of the model. Therefore, it is possible to distinguish between the obscuring effects of interparticle interference and changes of micellar size resulting from dilution. This is an important advantage of the X-ray small-angle scattering compared with other methods.

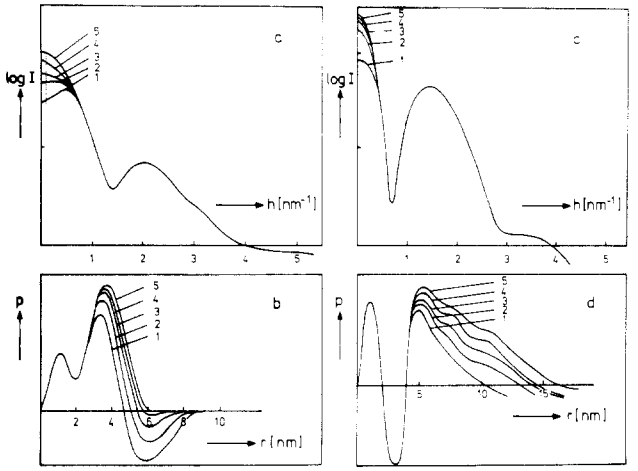

FIGURE 3: Experimental scattering and distance distribution functions (a and b, 3:1 micelles; *c* and *d*, 1:1 micelles) at different concentrations (1 = 10%, 2 = 5%, 3 = 2.5%, 4 = 1.25%, and 5 = extrapolation to zero concentration). The vertical dotted lines of parts a and c indicate the smallest measured scattering angle. Whereas an unambiguous determination of the maximum diameter is possible in the case of the 3:1 system, the unclear course of $p(r)$ beyond the intersection with the abscissa (this part has been left out in part d for this reason) prevents such an analysis in the case of the 1:1 micelles.

maintain the critical micellar concentration. This change in composition, however, produces only a negligible change of size. This was also proved by using a diluent containing bile

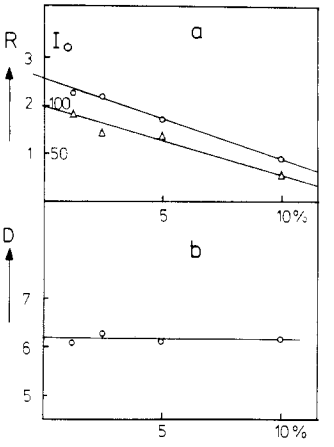

FIGURE 4: Concentration dependence of the radii of gyration (R) (circles) and the scattering intensity at zero angle I(0) (triangles) for the 3:1 (a) micelles. Part b shows the dependence of the maximum dimension D on the dilution.

salts close to their critical micellar concentration so that the release of bile salts from the micelles is suppressed. The results are practically identical.

Parts c and d of Figure 3 show the concentration dependence of the 1:1 micelle scattering curves and the corresponding $p(r)$ function. As previously mentioned, the scattering curve in the 1:1 case is less accurate than for the 3:1 case at smallest angles. Therefore, from the limited resolution according to the sampling theorem, the course of $p(r)$ at r values greater than 12 nm is not reliable, and it is difficult on the basis of the present data to determine exact values for the maximum dimension. It can be stated, however, that D for the 1:1 micelles is somewhat larger than 10 nm in a 10% (w/v) solution, and this increases rapidly upon dilution with 0.15 M NaCl. This is considered to be due to the change of the intramicellar mixing ratio from 1:1 to 0.75:1 which occurs when a 10% solution is diluted to 1.25% (for the critical micellar concentration of the physiological bile salt mixture, an estimated mean value was used for this calculation). As shown in Figure 7, the dimensions of the lecithin-rich micelles depend very strongly on the mixing ratio in contrast to those of the bile-salt-rich micelles.

Radius of Gyration. The radius of gyration, R, of a particle can be determined from the scattering data in two different ways, either by application of the Guinier approximation (Guinier & Fournet, 1955) or from the second moment of the distance distribution function, $p(r)$ (eq 3). Both methods were used in this study. The values obtained are shown in Figure 4 as a function of the concentration. In the case of the 3:1 micelles, the increase of R with dilution must be due exclusively to intermicellar interferences since particle size, D, as well as the particle shape were found to be constant in this range of concentrations. It is therefore possible to eliminate the concentration effect by extrapolation to zero concentration. This leads to a value for R of 2.5 ± 0.1 nm.

For the 1:1 micelles as discussed previously, the observed increase of R with dilution is certainly a composite effect resulting from a combination of interparticle interference effect and particle growth. As already indicated, it is not now possible to distinguish between these effects. We can only estimate that R for the 1:1 micelles will be in the range 5.0–6.0 nm and will increase with dilution, i.e., with increasing relative lecithin content up to values of 10 nm and more at the phase limit.

Since these micelles lack a homogeneous internal electron density distribution, R is only a measure of particle size if determined at infinite contrast (R_F). To accomplish this would

necessitate application of the contrast variation method (Stuhrmann, 1974). Unfortunately, this is not possible since we observed that all of the types of additives necessary for the purpose of contrast adjustment induce dramatic alterations in micellar structure.

However, we could demonstrate that the dependence of R on the contrast is small at the one contrast used for our measurements and that this is valid for all the structures shown in Figures 8 and 9.

From a detailed analysis taking into account the second moment of the electron density fluctuations (Stuhrmann, 1974), it can be estimated that the values of R determined experimentally will be about 5% and 10% higher than the theoretical values at infinite contrast (R_F) for the 3:1 and 1:1 systems, respectively. These are 2.4 nm (3:1) and 5.0 nm (1:1).

Particle Shape. A first approach to deriving the particle shape is to obtain the ratio D/R_F, which is a measure of isometry. This ratio is 2.58 for a sphere and increases with increasing axial ratio. For example, D/R_F of a flat circular cylinder with a diameter to height ratio of 3:1 is 2.87, and a prolate ellipsoid with a 5:1:1 axial ratio has a D/R_F value of 4.30. The experimental value for 3:1 bile salt/lecithin micelles is 2.6. This clearly indicates a high degree of isometry. This finding seems to be characteristic for all bile salt/lecithin mixed micelles with a bile salt content higher than 65 mol %.

The 1:1 system behaves quite differently. The value of ~2.8 for D/R_F clearly indicates considerable anisometry, which increases strongly upon shifting the mixing ratio toward higher lecithin content. This increase is obviously caused by an anisometric growth of the micelles. The same effect is also observed with dilution by addition of bile-salt-free solvent.

A refined and more detailed description of the micellar structure is possible now by comparison of the theoretical scattering functions calculated for model bodies with the experimental data. Knowledge of the internal structure is necessary, in order to reduce the number of possible models. The oscillation of the $p(r)$ function at r values around 3 nm indicates that the mean separation of the interfaces between the high and low electron density regions (polar head groups and apolar hydrocarbon compounds) is in the range of 3 nm.

The electron density distribution function $\rho(r)$ can be calculated from the scattering amplitudes by Fourier transformation. In the case of a particle with spherical symmetry, the radial electron density distribution $\rho(r)$ follows from

$$\rho(r) = \frac{1}{2\pi^2}\int_0^\infty F(h)h^2\frac{\sin hr}{hr}\,dh \qquad (9)$$

where $F(h)$ is the scattering amplitude which is $[i(h)]^{1/2}$.

It is also possible to calculate $\rho(r)$ by direct deconvolution of the three-dimensional distance distribution function $p(r)$ (O. Glatter, unpublished results). This method has the advantage that there are no problems with the determination of the phases (signs) of $[i(h)]^{1/2}$. In the present study, we applied both methods with essentially similar results.

For lamellar particles of constant thickness and infinite planar extension, the corresponding functions $p_t(r)$ and $\rho_t(r)$ can be derived from the thickness factor $i_t(h)$, which is equal to

$$i_t(h) = i(h)h^2 \qquad (10)$$

by the following relations:

$$p_t(r) = \frac{1}{\pi}\int_0^\infty i(h)h^2 \cos hr\,dh \qquad (11)$$

$$\rho_t(r) = \frac{1}{2\pi^2}\int_0^\infty F(h)h \cos hr\,dh \qquad (12)$$

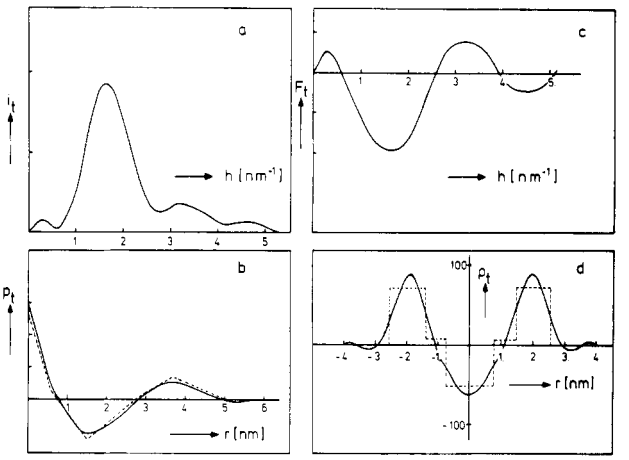

FIGURE 5: Evaluation of the thickness factor $i_t(h) = i(h)h^2$ for the 1:1 mixed micelles. Part a shows the thickness factor- and part c the corresponding amplitudes, $[i_t(h)]^{1/2}$. In (b) the real space $p_t(r)$ is shown as derived from the experimental data (full line). Part d exhibits the electron density distribution $\rho_t(r)$ across the bilayer. The dotted line represents the least-square step approximation to this experimental $\rho_t(r)$ (full line); the correlated $p_t(r)$ is compared with the experimental result in (b) (dotted line). The ρ values in (d) are given on an absolute scale.

Both the distance distribution function $p_t(r)$ and the electron density distribution function $\rho_t(r)$ contain only information about the one-dimensional structure across the plane of the bilayer.

In a manner similar to $\rho(r)$, $\rho_t(r)$ also can be obtained directly from $p_t(r)$ by a recently developed deconvolution method (O. Glatter, unpublished results). By analogy to eq 4, the integral over $p_t(r)$ equals the zero angle scattering intensity from the one-dimensional electron density profile

$$i_t(0) = \int_0^\infty p_t(r)\,dr \qquad (13)$$

The mass per unit area of the lamellae can then be calculated according to

$$M\ \text{nm}^{-2} = i_t(0)^{1/2}(\Delta z)^{-1} \qquad (14)$$

Since we wished to avoid introduction of any assumptions or biases to the interpretation of the structure of the micelles, we approached the evaluation of the 3:1 and the 1:1 micelles by assessment of two possible cases. Both the case of three-dimensional electron density inhomogeneity with radial symmetry and the one-dimensional case with bilayer-like structure were applied.

The outcome of this, however, was that reasonable results were obtained only when the 3:1 micelles were treated as centrosymmetric particles and the 1:1 micelles as bilayers. Conversely, with different treatment, only nonsensical information in the form of large-frequency oscillations of quite irrationally high levels was obtained for the distance function and electron density distribution function.

The results of the evaluations of the 1:1 micelles are summarized in Figure 5.

As is evident from Figure 5b, the thickness of the lamella is 5.1 nm since $p_t(r)$ remains essentially zero beyond this value. The electron density distribution function $\rho_t(r)$ was determined independently by two methods. First, direct calculations were made from the scattering amplitudes (Figure 5c) of the thickness factor (Figure 5a) using eq 13 and, second, calculations were made by an indirect iterative method. In the second approach, we optimized an arbitrary start function consisting of a number of step functions by changing both the height and the width of the steps in order to obtain an optimum

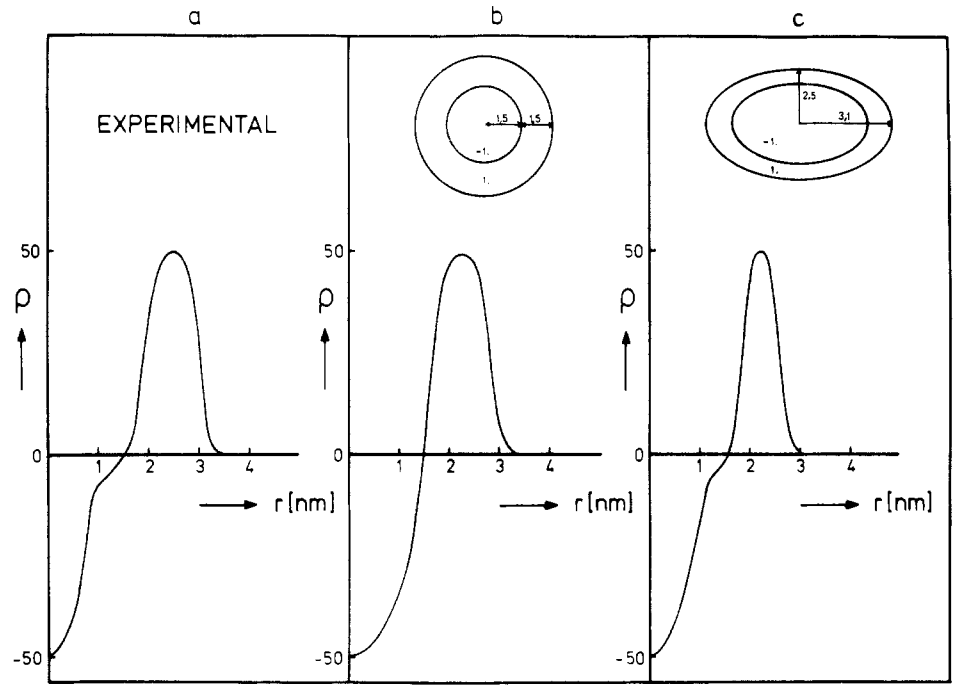

FIGURE 6: Comparison of the electron density distribution functions calculated from the experimental data of the 3:1 micelles (a) with two model bodies (b, c). As shown, slight deviations from sphericity do not essentially influence the resulting electron density distribution function calculated according to eq 9.

least-squares approximation to $p_t(r)$ after convolution (Program FOURSINC; Glatter, unpublished) (dotted lines in Figure 5b,d).

The functions $p_t(r)$ and $\rho_t(r)$ clearly indicate the following structural features: a typical bilayer-like arrangement with two outer layers of 1.0-nm thickness and an absolute electron density level of 390 e·nm^{-3} each, two intermediate layers of 0.7 nm and 340 e·nm^{-3}, and a central layer of 1.7 nm and 280 e·nm^{-3}. The mass per unit area of the layer is 1900 nm^{-2}.

For the 3:1 micelle system, a radial electron density distribution function was obtained by applying eq 9 to the three-dimensional structural amplitude (Figure 6). Accordingly, bile-salt-rich particles consist of a core of ~1.5-nm radius and 280–290 e·nm^{-3} electron density which is surrounded by a 1.5-nm shell of 380–390 e·nm^{-3}.

In order to reply the possible objection that the necessary conditions, i.e., ideal sphericity and infinite planar extension, for an exact application of eq 9 and 12 are not fulfilled by the present micelles, several simulations were carried out to assess the degree of potential error. Figure 6 shows the electron density distribution functions calculated from two different models when compared to the experimentally derived $\rho(r)$ for the 3:1 mixed micelles. Larger deviations from sphericity can be excluded with respect to the previously indicated anisometry factor of 2.6. This finding indicates that the core shell model, i.e., the essential outcome of the interpretation of $\rho(r)$, is not seriously undermined by such slight variations of shape.

By analogous simulations it can also be shown that application of eq 11 is justified when the lateral bilayer dimension is more than 2.5 times the bilayer thickness, which as demonstrated in the present work is the case for 1:1 micelles.

Discussion

The present results clearly indicate that there are two principles of structure for bile salt/lecithin mixed micelles. As indicated by the introduction, previous views had considered only a single discoid structure, valid for all mixing ratios. If we now consider how this model, a disk of lecithin bilayer surrounded by a ribbon of bile salts at its perimeter (Small, 1967), behaves as the bile salt:lecithin ratio increases, we shall see that it fails when tested against our new structural data.

We shall first discuss the dependence of the micelle molecular weight (M) and the maximum dimension (D) on the maximum number of bile salts (n_{BS}) which can surround a section of lecithin bilayer containing n_L molecules. If l is the thickness of a bile salt molecule and a is the area occupied by one lecithin molecule

$$n_{BS} = 2\frac{L}{l} = \frac{4\pi r}{l} = \frac{4\pi\sqrt{\frac{A}{\pi}}}{l} = \frac{4\sqrt{\frac{\pi a}{2}}n_L}{l}$$

or

$$n_{BS}^2 = \frac{8\pi a}{l^2}n_L \tag{15}$$

where A is the total area of the bilayer and L is its circumference. Also,

$$M = n_{BS}M_{BS} + n_L M_L \tag{16}$$

where M_{BS} is the molecular weight of one bile salt molecule and M_L is that of one lecithin molecule. By combining eq 16 and 17, one obtains

$$M = \frac{8\pi a}{l^2}\left[\frac{M_{BS}}{\left(\frac{n_{BS}}{n_L}\right)} + \frac{M_L}{\left(\frac{n_{BS}}{n_L}\right)^2}\right] \tag{17}$$

To a good approximation

$$n_{BS} = \frac{4\pi a M_{BS}}{l^2}\frac{1}{M} + \sqrt{\frac{8\pi a M_L}{l^2}}\frac{1}{\sqrt{M}} \tag{18}$$

(error less than 1.5% to M values as low as 10000 daltons, which are not seen with these mixed micellar systems). When a value of 490 for the mean molecular mass for a physiological mixture of bile salts as used for our experiments and values

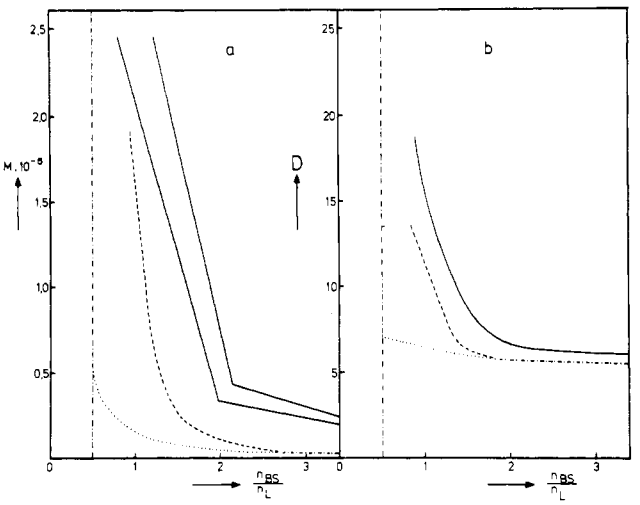

FIGURE 7: Dependence of the micellar mass M (a) and the maximum diameter D (b) of bile salt/lecithin mixed micelles on the mixing ratio. Full lines represent the X-ray small-angle scattering results (the two lines in (a) are due to the relative large error limits), dashed lines the mixed disk model, and dotted lines the model according to D. M. Small. The interrupted vertical line indicates the phase limit. A quite different aggregation behavior is observed beyond a mixing ratio of approximately 2:1. Whereas the mixed-disk model shows some similarity to the X-ray data for lecithin-rich micelles, particles predicted for bile-salt-rich systems from the mixed-disk as well as from the Small model are much too small.

of 770 for M_L, 0.5 nm^2 for a, and 1 nm for l are used, the functions plotted in Figure 7 are obtained. They predict M and D for a micelle constructed according to the Small model, without the assumption that free bile salt micelles would "coexist" with the mixed micelles. The experimentally observed values of M and D are much larger than predicted from the model at all mixing ratios, thus disproving this model at all bile salt/lecithin mixing ratios.

From a similar calculation and from measurements of the Stokes radius by quasi-elastic laser light scattering, Mazer et al. (1977) were lead by deduction to a different model, in which bile salts were not only situated at the micelle perimeter but also incorporated into the bilayer. Good agreement between predicted and experimental radii were found for bile salt to lecithin ratios smaller than 2 by using this "mixed disk" model. To get agreement at bile salt to lecithin ratios exceeding the value of 2, it was postulated that the excess bile salt molecules which for steric reasons could not be accommodated by the mixed micelle would form simple bile salt micelles "coexisting" with the mixed micelles. The mixed micelle in this construct was thought to take the mixed-disk form at all molar ratios with a constant internal mixing ratio similar to the phase limit of the two compounds. It is evident that the results of the present work are not compatible with this model for bile salt to lecithin ratios greater than 2. In our view, it must be generally very difficult to derive trustworthy structural information from any given single parameter, in this case, the diffusion coefficient. This is because of the superimposed influence of various terms including particle size, particle shape, intermicellar forces, solvent interactions, and polydispersity afflicting uncertainties on the evaluation of the diffusion coefficient measurement.

The validity of the mixed-disk model at higher BS-L molar ratios is open to challenge by reason of another simple consideration. According to the calculated dimensions for the mixed-disk model and in agreement with the laser light-scattering measurements, Mazer et al. (1977) found the disk radius of a 3:1 mixed micelle formed by sodium taurodeoxycholate and egg-yolk lecithin to be 7.5 Å. Assuming a bilayer thickness of 5 nm (Figure 8 of the paper cited above), this would correspond to a bilayer area of 1.7 nm^2 and, consequently, to one molecule of lecithin "mixed" with three bile salt molecules in each half of the mixed disk. In the case of a 2:1 mixing ratio, for which these authors believe that pure bile salt micelles no longer coexist with mixed disk micelles, four lecithin molecules would be mixed with eight bile salt molecules in each half of the bilayer. In our view, such a small number of molecules cannot likely form a stable bilayer arrangement. With increasing lecithin content, however, this model becomes very likely and, in addition, is compatible with our X-ray data.

The influence of polydispersity on the present XSAS results is another important issue. This is in light of the putative "coexistence" of simple bile salt micelles in bile-salt-rich mixed systems (>2:1 BS/L) from the recent laser light-scattering studies. In order to get an estimate of the polydispersity effect, a series of computer simulations were carried out. These were designed to test the validity for possible coexistence of pure excess bile salt micelles with bile-salt-rich mixed micelles, coexistence of pure bile salt micelles with mixed bilayer micelles, and coexistence of bile-salt-rich and lecithin-rich mixed micelles. In all cases, a variety of mixing ratios were chosen, taking into account the above-described geometrical considerations. Scattering curves were calculated for these systems considering the individual scattering power of the coexisting micelle types. In order to make these calculated curves comparable to the experimental ones, they were artificially afflicted with statistical noise, background scattering, and collimation errors and then treated in the same way that the experimental scattering functions were derived.

Similarly, when a recently developed computer program was used (Glatter, 1980), various types of size distribution were considered. From this evidence taken together, we can conclude that the phenomena of coexistence as well as even a spectrum of size distribution, if it is real, occur at levels far below the requirements that permit a correct evaluation of X-ray scattering data. The only point which cannot on this basis be excluded relates to a distribution in the lateral dimensions of the bilayer micelles. In all the other cases, the simulated curves differ significantly from the experimental ones.

We now attempt a refined structural description of the micelles on the basis of geometrical models.

For both the 1:1 and for the 3:1 system, five different types of arrangement were simulated. The dimensions and electron density levels were selected in accordance with the experimental findings and then adjusted in order to obtain an optimum fit for scattering from each type of model to the experimental curves.

For the 1:1 system, this comparison is shown in Figure 8, where a represents the mixed disk (homogeneous mean electron density along the plane of the layer), b is the Small model (high electron density ribbon at the perimeter), c is a hypothetical vesicle model (spherical bilayer with 5-nm thickness), and d and e are other alternative structures, which, in principle, are possible.

From the scattering functions, but more clearly from the real space distance distribution functions, an unambiguous decision in favor of the mixed disk is possible. All other structures including the Small model give results widely different from the experimental data.

The bilayer thickness of 5.1 nm which had previously been derived from $p_t(r)$ and $\rho_t(r)$ is moreover directly supported by the second maximum of $p(r)$ at 5.1 nm. Since this maximum

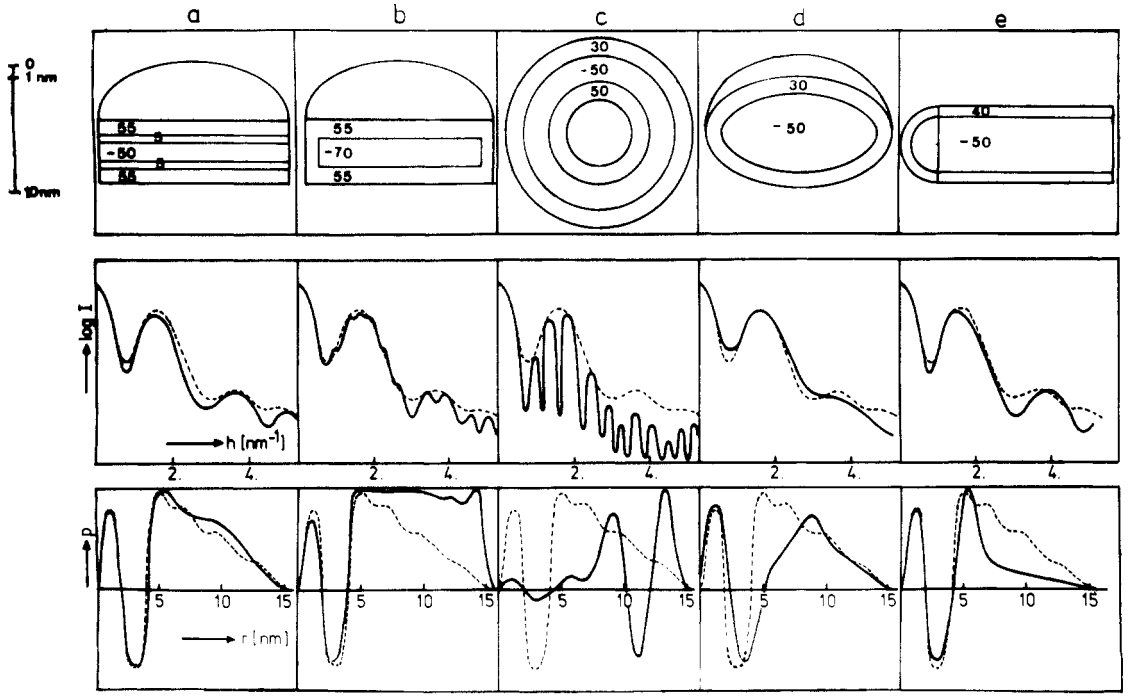

FIGURE 8: Comparison of some significant possible models for the 1:1 mixed micelles. (a) Mixed-disk model; (b) bilayer model with bile-salt ribbon; (c) vesicle model; (d) prolate ellipsoid; (e) cylindrical model. The dotted lines are the experimental functions. The models are those of optimum fit for the various structural configurations. The dimensions in nanometers are marked by the bar; electron density levels are given in relative units.

has been reproducibly found at exactly the same position, this value may be considered as the most accurate value in the entire present study.

Whereas bilayers formed by pure egg-yolk lecithin were found to have a smaller thickness (Small, 1966b), the value obtained here is exactly the same as for the abnormal plasma lipoprotein LpX associated with cholestasis (Laggner et al., 1977). This could be of importance because it has been reported (Manzato et al., 1976; Seidel, 1977) that the major macromolecular complex of bile can be directly converted into vesicular LpX by addition of serum or serum albumin, respectively. Of related interest is our finding that biliary mixed micelle systems can take the form of vesicles under certain not yet completely defined conditions.

The interpretation in molecular terms of the electron density distribution for a bilayer is reasonably straightforward. The polar heads of lecithin and bile salt form the outer layers of high electron density. The middle regions of medium electron density are formed by a mixture of sterol rings of the bile salts with the fatty acid chains of lecithin. By calculating this density from the individual partial specific volumes and electron concentrations of both compounds, one obtains practically the same value as found experimentally. In the interior, only hydrocarbon chains of low electron density are present. There is also excellent agreement between the theoretical (280 e·nm^{-3}) and the experimental values.

Only the electron density of the outer layer which is in contact with the solvent differs from the theoretical value for unhydrated polar heads (480 e·nm^{-3}). From the experimental value of 390 e·nm^{-3}, we must conclude that 50–60% of the volume of this outer layer is occupied by solvent. It cannot be decided by this approach whether the middle regions of the micelle are also hydrated. This is because the sterol system (380 e·cm^{-3}) and the hydrocarbon chains have an average electron density of 337 e·nm^{-3} in a 1:1 mixture which is almost indistinguishable from the value for the solvent, 334 e·nm^{-3} (37 °C).

That there could also be considerable hydration of deeper regions (hydroxyl groups of the bile salts) in addition to the highly hydrated particle surface layer might be deduced from the particle volume when calculated from the molecular weight

$$V[\mathrm{nm}^3] = \frac{M\phi_2' \times 10^{21}}{N_A} \times 380\ \mathrm{nm}^3 \qquad (19)$$

The volume of the model in Figure 8a is about 700 nm^3, so that only about 55% of this space is filled with lipids. From the molecular weight we can also derive the area per lipid molecule by dividing the area of the lamella by half the aggregation number (200 + 200). A value of 0.7 nm^2 is found. This is proved by the mass per unit area (1900 nm^{-2}), which in contrast to M is essentially independent of the course of the scattering curve at very small angles. Since the mean molecular mass of one lipid molecule in a 1:1 mixture of bile salt and lecithin is 630, there are 1900 nm^{-2}/2 × 630 = 1.5 molecules/nm^2, or 0.66 nm^2/molecule.

This high specific area also indicates a high degree of hydration. Quantitatively it can be estimated that on an average each lipid molecule is associated with 28 water molecules. We cannot assign individual hydrations to bile salt or lecithin nor distinguish between bound and free water.

A molecular model of the 1:1 micelle is presented in Figure 10. For the 3:1 micelle, the differences between the models shown in Figure 9 give rise to only small differences in scattering and $p(r)$ curves. This is because no dominating structural principle exists similar to the thickness factor for the 1:1 bilayer-like micelles. Therefore, it is difficult to decide in favor of one or the other of the models shown in Figure 9 merely on the basis of the XSAS data. But we can rule out some of these models from other considerations.

Models a and b of Figure 9 are bilayers. If we assume the bilayer thickness to be 5.1 nm as found for the 1:1 system, however, the model disagrees strongly with the observed high isometry of 3:1 micelles. On the other hand, if we make the bilayer isometric by adjusting the thickness to 4.4 nm, this is

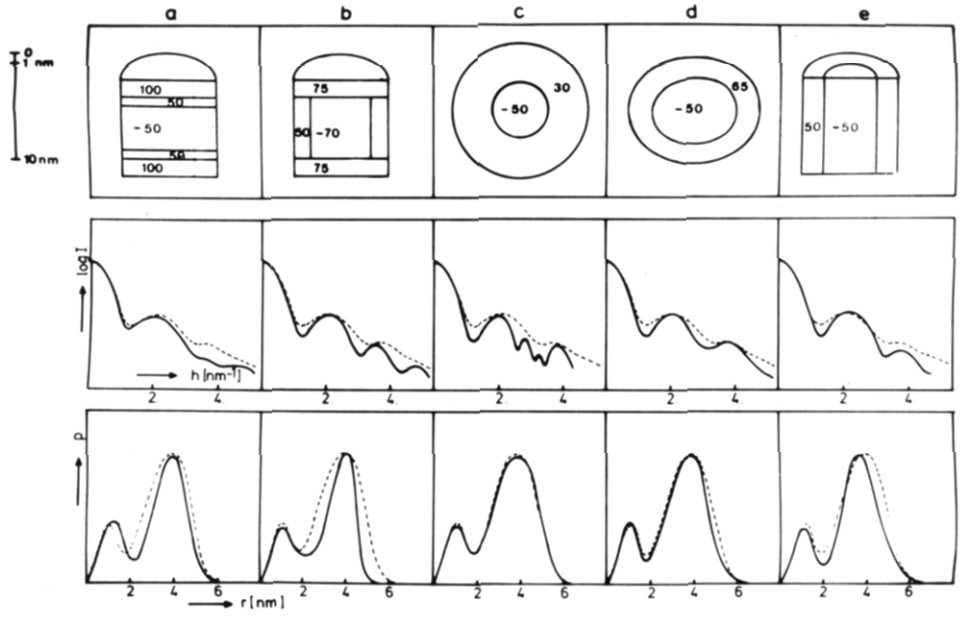

FIGURE 9: Comparative survey of some possible models for the 3:1 mixed micelles (analogous to Figure 8).

incompatible with the observed thickness of a mixed bile salt–lecithin bilayer. Furthermore, it cannot be expected that a stable bilayer arrangement is formed by only 12 lecithin molecules. (The aggregation number of 3:1 micelles is 36 bile salt and 12 lecithin molecules.) In view of these arguments, the deviations of the model scattering and $p(r)$ functions from the experimental data are considerably more important than they otherwise may seem. In turn, the better agreement of models c and d (Figure 9) becomes more significant when the following observations are taken into account.

Pure bile salts have been found to form radially symmetrical micelles, the size and shape of which are only a little influenced by lecithin incorporation up to the critical mixing ratio; 3:1 micelles are thus best regarded as a rather small perturbation of this structure.

In addition, valuable supplementary information was obtained from electron spin resonance spectroscopic data (K. Müller, unpublished results). This confirms the view that there are two different principles of lipid arrangement in the 3:1 and 1:1 micelles. In lecithin-rich systems, increasing hydrocarbon chain mobility was found as the spin-label was moved toward the center of the micelle, a characteristic of bilayers generally. In bile-salt-rich micelles, the opposite was observed. The order parameter was higher the closer the spin-label was to the center, which is a unique finding. This is an indication of dense packing in the core of a radially arranged particle.

Although it is difficult to exclude model 9e, it seems most likely that the 3:1 micelle, in fact, represents a nearly spherical particle. There is a slight deviation toward an ellipsoid with an axial ratio of 1.2:1.1:1 for which an optimum fit to the experimental data was achieved. The longest diameter is 6.2 nm. Figure 10 (lower) shows the molecular arrangement of the 3:1 micelle that seems most probable from all our lines of evidence.

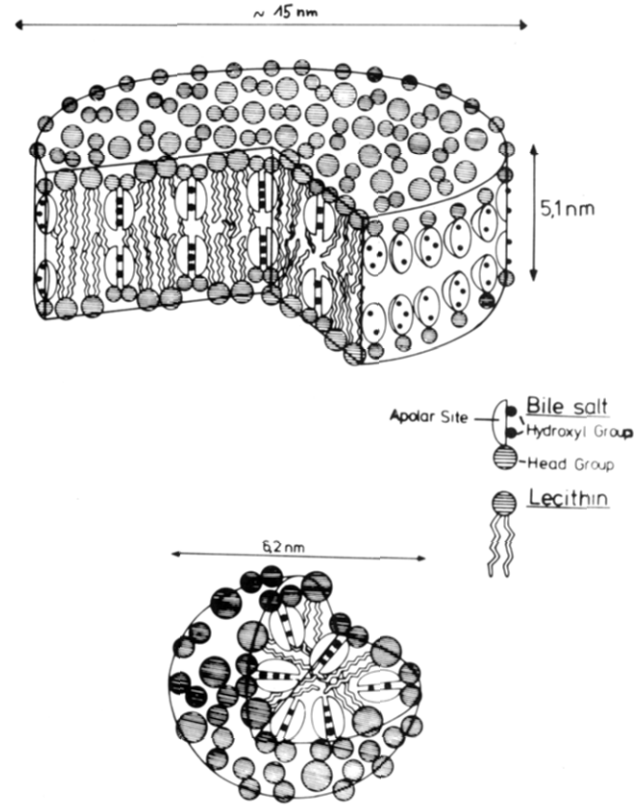

FIGURE 10: Molecular models for the lecithin-rich type of mixed micelles (top) and for the bile-salt-rich type (bottom). The bile salts are thought to form pairs to avoid contact of the hydroxyl groups (solid circles) with the apolar environment.

Summary and Conclusions

There are two different types of micelles, depending on the molar ratio of bile salt to lecithin. Lecithin-rich micelles have the mixed-disk structure, but bile-salt-rich micelles are isometrical particles. The translation between the two types takes place at a molar ratio of about 2:1. Claffey & Holzbach (1981) from measurements of the UV absorption and thermotropic behavior of these systems, using taurochenodeoxycholate as the bile salt, found that the transition occurs at 1.8:1.

Bile-salt-rich micelles are characterized by their centrosymmetric arrangement of molecular constituents and almost spherical overall shape. Their size is only minimally dependent upon the mixing ratio. While the lecithin content is increased from 10 to 30 mol %, the diameter increases only from 6.0 to 6.4 nm and the micellar mass only from 20 000 to 35 000 daltons. The particle shape remains constant. In addition, no measurable concentration dependence for size and shape

is observed. *Lecithin-rich* micelles, by contrast, are disk-shaped bilayers of 5.1-nm thickness. Bile salts and lecithin are homogeneously distributed over the entire micelle. The micellar mass increases sharply from 40 000 to several hundred thousand daltons when the lecithin content is increased from 35 to 60 mol %. The diameter of the disk increases from less than 10 to more than 50 nm. Micellar size is very sensitive to changes in concentration.

In human bile, the molar ratio is such as to warrant the assumption that micelles take the centrosymmetric form, provided that the characteristic structural behavior of the model systems as reported here is not changed by the other bile constituents. If the assumption is valid, this observation suggests a control mechanism for cholesterol solubilization by bile, given only that cholesterol solubilization properties are different for each micelle type under physiological conditions. This would explain why biliary supersaturation defined by phase diagrams for model solutions frequently fails to result in cholesterol precipitation. It may be necessary to define supersaturation not only with regard to total lipid concentration, as done by Carey & Small (1978), but also with regard to other factors which may control the transition between bilayer and globular micelles.

Acknowledgments

I am indebted to Dr. R. Thomas Holzbach for helpful discussions which stimulated this work, for providing chemicals, and for protocols for the preparation of study samples. Katharina Scharf provided expert technical assistance.

References

Admirand, W. H., & Small, D. M. (1968) *J. Clin. Invest. 47*, 1043–1052.

Bourgès, M., Small, D. M., & Dervichian, D. G. (1967) *Biochim. Biophys. Acta 144*, 189–201.

Carey, M. C., & Small, D. M. (1970) *Am. J. Med. 49*, 590–608.

Carey, M. C., & Small, D. M. (1978) *J. Clin. Invest. 61*, 998–1026.

Casassa, E. F., & Eisenberg, H. (1964) *Adv. Protein Chem. 19*, 387–394.

Chavez, M. H., & Krone, C. L. (1976) *J. Lipid Res. 17*, 545–547.

Claffey, W. J., & Holzbach, R. T. (1981) *Biochemistry* (following paper in this issue).

Dervichian, D. G. (1968) *Adv. Chem. Ser. No. 84*, 78–87.

Fontell, K. (1971) *Kolloid Z. Z. Polym. 246*, 710–718.

Gähwiller, Ch., von Planta, C., Schmidt, D., & Steffen, H. (1977) *Z. Naturforsch. B: Anorg. Chem., Org. Chem., Biochem., Biophys., Biol. 32*, 748–755.

Glatter, O. (1977) *J. Appl. Crystallogr. 10*, 415–421.

Glatter, O. (1979a) *J. Appl. Crystallogr. 12*, 166–175.

Glatter, O. (1980) *J. Appl. Crystallogr. 13*, 7–11.

Grundy, S. M., Metzger, A. L., & Adler, R. D. (1972) *J. Clin. Invest. 51*, 3026–3043.

Guinier, A., & Fournet, G. (1955) in *Small-Angle Scattering of X-Rays*, Wiley, New York.

Hofmann, A. F., & Small, D. M. (1967) *Annu. Rev. Med. 18*, 333–376.

Holzbach, R. T., Marsh, M., Olszewski, M., & Holan, K. (1973) *J. Clin. Invest. 52*, 1467–1479.

Ingelfinger, F. J. (1968) *Gastroenterology 55*, 102–104.

Jánosi, A., & Degovics, G. (1976) *Intern. Publ. Inst. Röntgenfeinstrukturforsch. (Graz) 4*, 1–17.

Kratky, O. (1954) *Z. Elektrochem. 58*, 49–53.

Kratky, O. (1958) *Z. Elektrochem. 62*, 66–74.

Kratky, O. (1963) *Prog. Biophys. Mol. Biol. 13*, 105–173.

Kratky, O., & Skala, Z. (1958) *Z. Elektrochem. 62*, 73–77.

Kratky, O., Leopold, H., & Stabinger, H. (1973) *Methods Enzymol. 27D*, 98–110.

Kupke, D. W. (1973) *Principles and Techniques of Protein Chemistry, C*, pp 1–75, Academic Press, New York.

Laggner, P., & Müller, K. (1978) *Q. Rev. Biophys. 11*, 371–425.

Laggner, P., Glatter, O., Müller, K., Kratky, O., Kostner, G., & Holasek, A. (1977) *Eur. J. Biochem. 77*, 165–171.

Lee, J. A., & Timasheff, S. N. (1974) *Biochemistry 13*, 257–265.

Leopold, H. (1969) *Elektronik 11*, 350–351.

Luzzati, V. (1960) *Acta Crystallogr. 13*, 939–945.

Manzato, E., Fellin, R., Baggio, G., Walch, S., Neubeck, W., & Seidel, D. (1976) *J. Clin. Invest. 57*, 1248–1260.

Mazer, N. A., Kwasnick, R. F., Carey, M. C., & Benedek, G. B. (1977) *Micellization, Solubilization, Microemulsions, Proc. Int. Symp. 1*, 383–402.

Müller, K., Laggner, P., Glatter, O., & Kostner, G. (1978) *Eur. J. Biochem. 82*, 73–90.

Neiderhiser, D. H., & Roth, H. P. (1968) *J. Clin. Invest. 47*, 1043–1052.

Nilsson, S., & Scherstén, T. (1969) *Gastroenterology 57*, 525–532.

Northfield, T. C., & Hofmann, A. F. (1975) *Gut 16*, 1–17.

Oh, S. Y., McDonnell, M. E., Holzbach, R. T., & Jamieson, A. M. (1977) *Biochim. Biophys. Acta 488*, 25–35.

Seidel, D. (1977) *Klin. Wochenschr. 55*, 611–623.

Shaffer, E. A., & Small, D. M. (1977) *J. Clin. Invest. 59*, 828–840.

Shankland, W. (1970) *Chem. Phys. Lipids 4*, 109–130.

Shankland, W. (1977) *Chem. Phys. Lipids 19*, 20–42.

Small, D. M. (1967) *Gastroenterology 52*, 607–610.

Small, D. M., & Rapo, S. (1970) *New Engl. J. Med. 283*, 53–57.

Small, D. M., Bourgès, M., & Dervichian, D. G. (1966a) *Biochim. Biophys. Acta 125*, 563–580.

Small, D. M., Bourgès, M., & Dervichian, D. G. (1966b) *Nature (London) 211*, 816–818.

Small, D. M., Penkett, S. A., & Chapman, D. (1969) *Biochim. Biophys. Acta 176*, 178–189.

Stabinger, H., & Kratky, O. (1979) *Makromol. Chem.* (in press).

Stevens, R. D. (1977) *J. Lipid Res. 18*, 417–422.

Stuhrmann, H. B. (1974) *J. Appl. Crystallogr. 7*, 173–178.

Vlahcevic, Z. R., Bell, C. C., Jr., Bohac, I., Farrar, J. T., & Swell, L. (1971) *Gastroenterology 59*, 165–173.